BASIC SCIENCE

Cardiac magnetic resonance and electroanatomical mapping of acute and chronic atrial ablation injury: a histological validation study

James L. Harrison[1,2]*, **Henrik K. Jensen[3]**, **Sarah A. Peel[1]**, **Amedeo Chiribiri[1,2]**, **Anne K. Grøndal[4,5]**, **Lars Ø. Bloch[3,5]**, **Steen F. Pedersen[4]**, **Jacob F. Bentzon[3,6]**, **Christoph Kolbitsch[1]**, **Rashed Karim[1]**, **Steven E. Williams[1,2]**, **Nick W. Linton[1,2]**, **Kawal S. Rhode[1]**, **Jaswinder Gill[1,2]**, **Michael Cooklin[2]**, **C.A. Rinaldi[1,2]**, **Matthew Wright[1,2]**, **Won Y. Kim[3,5]**, **Tobias Schaeffter[1]**, **Reza S. Razavi[1]**, and **Mark D. O'Neill[1,2]**

[1]Division of Imaging Sciences & Biomedical Engineering, Medical Engineering Centre, King's College London, 3rd Floor, Lambeth Wing, St Thomas' Hospital, SE1 7EH London, UK; [2]Department of Cardiology, Guy's and St. Thomas' NHS Foundation Trust, London, UK; [3]Department of Cardiology, Aarhus University Hospital Skejby, Aarhus, Denmark; [4]Department of Cardiothoracic and Vascular Surgery, Aarhus University Hospital Skejby, Aarhus, Denmark; [5]MR-Center, Aarhus University Hospital Skejby, Aarhus, Denmark; and [6]Department of Clinical Medicine, Aarhus University, Aarhus, Denmark

See page 1436 for the editorial comment on this article (doi:10.1093/eurheartj/ehu061)

Aims	To provide a comprehensive histopathological validation of cardiac magnetic resonance (CMR) and endocardial voltage mapping of acute and chronic atrial ablation injury.
Methods and results	16 pigs underwent pre-ablation T2-weighted (T2W) and late gadolinium enhancement (LGE) CMR and high-density voltage mapping of the right atrium (RA) and both were repeated after intercaval linear radiofrequency ablation. Eight pigs were sacrificed following the procedure for pathological examination. A further eight pigs were recovered for 8 weeks, before chronic CMR, repeat RA voltage mapping and pathological examination. Signal intensity (SI) thresholds from 0 to 15 SD above a reference SI were used to segment the RA in CMR images and segmentations compared with real lesion volumes. The SI thresholds that best approximated histological volumes were 2.3 SD for LGE post-ablation, 14.5 SD for T2W post-ablation and 3.3 SD for LGE chronically. T2-weighted chronically always underestimated lesion volume. Acute histology showed transmural injury with coagulative necrosis. Chronic histology showed transmural fibrous scar. The mean voltage at the centre of the ablation line was 3.3 mV pre-ablation, 0.6 mV immediately post-ablation, and 0.3 mV chronically.
Conclusion	This study presents the first histopathological validation of CMR and endocardial voltage mapping to define acute and chronic atrial ablation injury, including SI thresholds that best match histological lesion volumes. An understanding of these thresholds may allow a more informed assessment of the underlying atrial substrate immediately after ablation and before repeat catheter ablation for atrial arrhythmias.
Keywords	Magnetic resonance • Atrial fibrillation • Ablation • Histology • Electroanatomical mapping

Introduction

Left atrial (LA) radiofrequency (RF) catheter ablation, of which pulmonary vein isolation (PVI) is the cornerstone, is a widely practised procedure for the treatment of atrial fibrillation (AF).[1] However, it is now apparent that acute achievement of PVI is seldom durable, which has refocused the field on the mechanisms of RF injury in the LA. In turn, there has been a recent increase in the use of cardiac

---

magnetic resonance (CMR) to provide pre- and post-procedural non-invasive atrial tissue characterization to assess patient suitability and response to catheter ablation,[2–11] and to guide both repeat catheter ablation[8,12] and real-time CMR-guided electrophysiology procedures.[13–16]

The use of CMR to characterize acute and chronic ventricular myocardial injury only became clinically accepted and in widespread use following comprehensive pathological validation,[17] yet there has been no fundamental validation work on the CMR assessment of the atrium. This is of particular importance as controversy remains regarding the reproducibility and diagnostic ability of atrial CMR.[18] Validation of atrial CMR necessitates defining signal intensity (SI) thresholds, which can distinguish between healthy and injured atrial tissue, rather than arbitrarily chosen SI thresholds used in clinical studies to date.[2,3,5,6,8–10]

Furthermore, invasive atrial endocardial voltage mapping, the current clinical gold standard for characterizing the atrial substrate, has not been pathologically validated or systematically compared with CMR findings. Voltage thresholds in common clinical use have been extrapolated from ventricular studies comparing electroanatomical mapping (EAM) with post-myocardial infarction scar[19,20] and not ablation-induced injury.

This study seeks to provide a comprehensive histopathological validation of CMR and endocardial voltage mapping of acute and chronic atrial ablation injury and to define SI thresholds for T2-weighted (T2W) and late gadolinium enhancement (LGE) CMR immediately following and 8 weeks after linear RF ablation in the porcine right atrium (RA).

Methods

Animal model and protocol

Animal studies complied fully with Danish law on animal experiments. Eight female Danish Landrace pigs (39 ± 1.8 kg) and eight female Göttingen mini-pigs (31 ± 2.9 kg) were pre-sedated with intramuscular azaperone (4 mg/kg) and midazolam (0.5 mg/kg). General anaesthesia was induced with intravenous ketamine (5 mg/kg) and midazolam (0.5 mg/kg), and the animals were intubated and mechanically ventilated. Anaesthesia was maintained with a continuous intravenous infusion of propofol (3 mg/kg/h) and fentanyl (15 mcg/kg/h).

The eight pigs underwent pre-ablation CMR, followed by EAM and ablation according to the protocols described below. These animals were then immediately transferred for post-ablation CMR according to the same protocol, before they were euthanized with intravenous phenobarbital (80 mg/kg).

The eight mini-pigs underwent the same protocol but were recovered from anaesthesia after post-ablation CMR and returned to the farm for 8 weeks. Mini-pigs were used as there was minimal growth during the recovery period. After 8 weeks, these animals were anaesthetized and underwent chronic CMR and EAM before being euthanized.

Electroanatomical maps and ablation

Two 8F sheaths were placed percutaneously in the right femoral vein, followed by an intravenous injection of 100 IU/kg heparin. Fluoroscopy was used to position a 6F decapolar reference catheter in the coronary sinus (CS). An 8F ablation catheter (Thermocool SF, D curve, Biosense Webster, Diamond Bar, CA, USA) was advanced to the RA. A 3D geometry of the RA was created using CartoXPress (Biosense Webster,

Diamond Bar, CA, USA) and a high-density pre-ablation peak-to-peak bipolar voltage map was constructed during proximal CS pacing. Linear RF ablation (25 W, 38°C, 8 mL/min irrigation) was performed from the superior vena cava (SVC) to the inferior vena cava (IVC) along the posterior wall of the RA. Ablation was performed as a continuous drag with the catheter moved every 30 s. Following completion of the intercaval linear lesion, a second high-density post-ablation voltage map was immediately acquired during proximal CS pacing. Continuity of the intercaval lesion was confirmed by the presence of double potentials along the line, absence of pace capture and the presence of a new activation detour during CS pacing. Chronic voltage maps were created in the same way but without ablation.

Cardiac magnetic resonance

Cardiac magnetic resonance was performed on a 1.5 T MR system (Achieva, Philips Medical Systems, Best, The Netherlands) and a five-element cardiac phased array coil. First, survey and sensitivity encoding reference scans were obtained, followed by a 2D multi-cardiac phase cine scan acquired in a four-chamber orientation. From this scan, the trigger delay was determined for all subsequent scans in order to minimize artefacts from atrial wall motion.

Sagittal T2W images were acquired [multi-slice turbo spin echo with a double inversion recovery pre-pulse and spectral pre-saturation with inversion recovery fat suppression; effective echo time (TE) = 45 ms; repetition time (TR) = twice the cardiac cycle length; spatial resolution = 1.5×1.5 mm^2 (reconstructed to 1.0×1.0 mm); slice thickness = 3 mm] using the respiratory navigator to minimize motion artefacts and to ensure acquisition at end-expiration for all slices.

Twenty minutes after administration of 0.2 mL/kg Gadovist (Bayer HealthCare Pharmaceuticals, Berlin, Germany), axial 3D LGE imaging was performed [respiratory-navigated, ECG-triggered inversion recovery turbo field echo acquisition; spatial resolution = $1.3 \times 1.3 \times 4$ mm^3 (reconstructed to $0.6 \times 0.6 \times 2$ mm^3); TE/TR = 3.0/6.2 ms; flip angle = 25°]. The inversion time was determined using a preceding Look-Locker sequence to achieve optimal suppression of ventricular myocardium.

Macroscopic and microscopic examination

After the animals were euthanized, the hearts were explanted and the RA was opened and photographed. The hearts were then fixed in formaldehyde. Next, the ablation line and surrounding tissue were excised *en bloc* and cut into 4 mm sections perpendicular to the ablation line. Each cross section was photographed and then dehydrated, embedded in paraffin, sectioned (3 μm sections), and stained with haematoxylin and eosin or Masson's Trichrome for microscopic examination.

Data analysis

Electroanatomical maps

Pre-ablation, post-ablation, and chronic voltage maps were exported from CartoXPress and imported into software custom-written with Matlab (The Mathworks, Natick, MA, USA). Axial slices were placed on the voltage maps at 4 mm intervals along the ablation line. For each slice, the centre of the ablation line was identified by minimizing the weighted distance to the ablation points (*Figure 1*). For the chronic voltage maps, which unavoidably had a different anatomical shell from the pre-/post-ablation maps, 'ablation points' were added manually to the estimated centre of the low-voltage zone to represent the ablation line. A graph of endocardial voltage against distance from the centre of the ablation line (from −25 to +25 mm) was constructed for each slice.
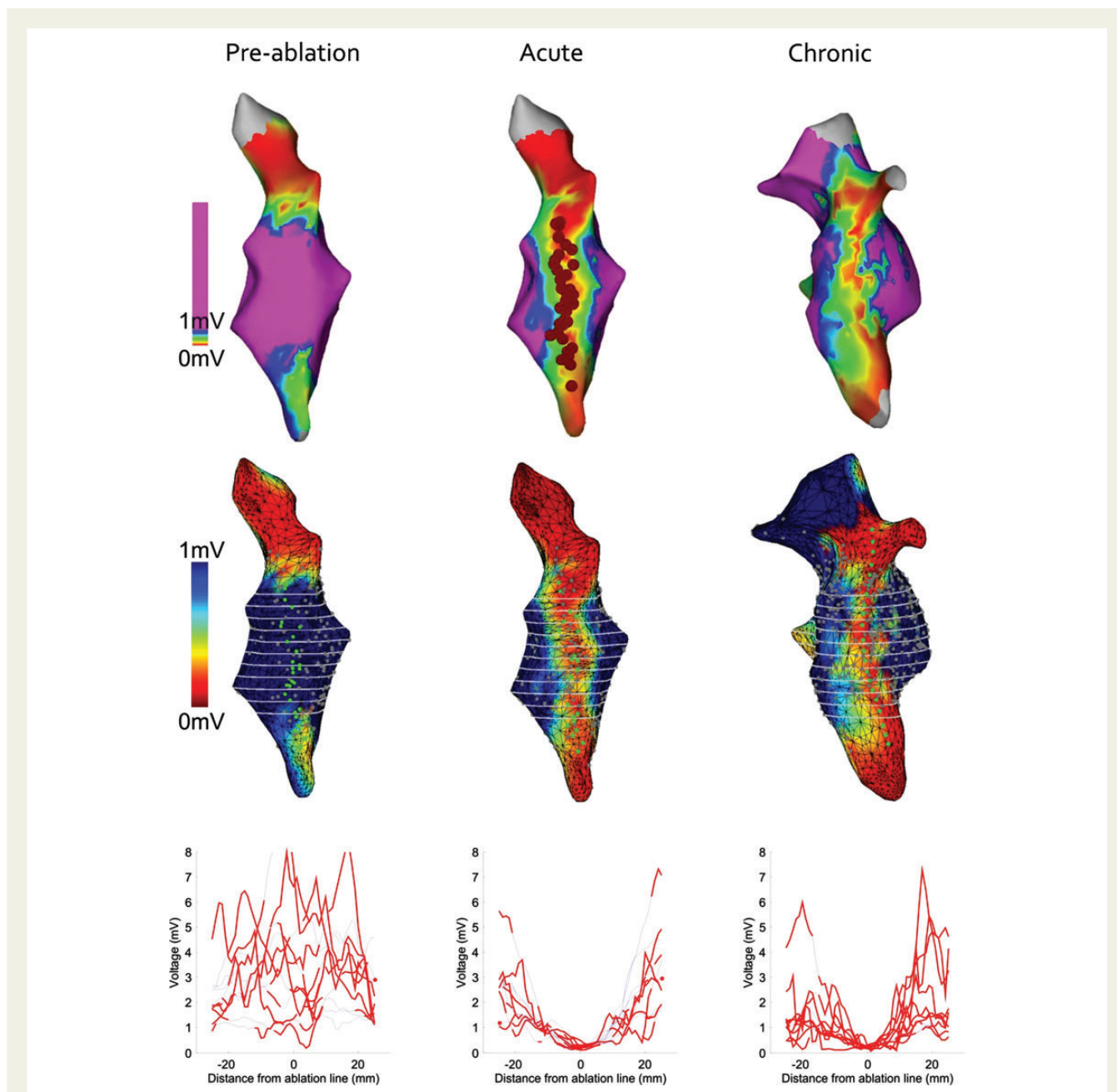
Figure 1 Electroanatomical mapping. Top row: CartoXPress endocardial bipolar voltage maps in a posteroanterior view (all from the same animal). Red circles indicate the site of linear radiofrequency ablation from the SVC to the IVC. Middle row: the same voltage maps have been imported in Matlab and reconstructed. Green circles indicate the site of ablation. Grey circles indicate data sampling points. Axial slices in white are shown at 4 mm intervals along the ablation line. Bottom row: graphs of endocardial voltage against distance from the centre of the ablation line (from −25 to +25 mm) for each axial slice. Red and blue lines indicate that values are ≤3 mm (non-interpolated) and ≥3 mm (interpolated) from a grey data sampling point, respectively. Only non-interpolated values were used for summary analysis in *Figure 3*.

Cardiac magnetic resonance

Pre-ablation, post-ablation, and chronic T2W and LGE images were analysed using 3D medical image segmentation software (itk-SNAP Version 2.2.0). First, two blinded expert observers independently selected a reference region (left ventricular (LV) myocardium for T2W and the atrial blood pool for LGE images) and the mean (and SD) SI for the reference region was calculated. Next, the two observers manually segmented the RA wall in the 3D volume by consensus (*Figure 2A*). Thresholds from 0 to 15 SD (at 0.1 intervals) above the reference SI were applied to the RA wall. A 3D segmentation was created for each threshold (where all pixels above the threshold SI were included in the segmentation) and the volume of the segmentation plotted against the SI threshold (*Figure 2B*).

Macroscopic examination

Using ImageJ image processing software (National Institutes of Health), two blinded expert observers manually segmented the total area of
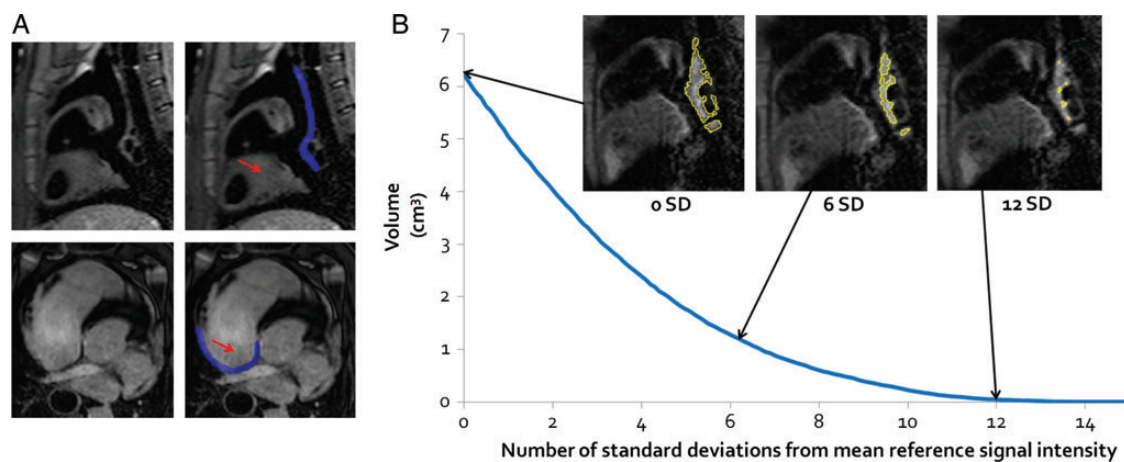
Figure 2 Cardiac magnetic resonance image analysis. (*A*) Sagittal T2-weighted (top row) and axial late gadolinium enhancement (bottom row) cardiac magnetic resonance images. The red arrows indicate the reference region against which signal intensities were compared (left ventricular myocardium for T2-weighted and the atrial blood pool for late gadolinium enhancement images). The blue overlay indicates the region segmented as the right atrium wall (in this particular slice). These images are all pre-ablation, but the same technique was used for all image analyses. (*B*) A graph for one post-ablation T2-weighted image of segmentation volume against the signal intensity threshold (expressed as the number of SD above the reference signal intensity). Sample images are included to show the segmentation created (outlined in yellow) at 0, 6, and 12 SD above the reference signal intensity.
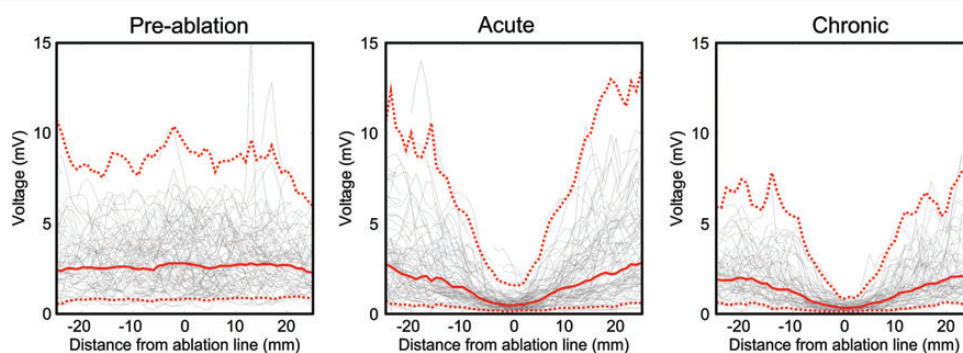
Figure 3 Voltage distribution across the ablation line. Average results for the 16 pre-ablation (left), 16 post-ablation (middle), and 8 chronic (right) electroanatomical maps. The solid red line indicates the mean, while the dashed red lines indicate the 95% confidence interval. Black lines indicate the raw data for all of the animals.

injury for each 4 mm cross-section on the gross pathological digital photographs taken after fixation in formalin, but before dehydration and staining for histological examination. For the acute specimens, the ablation lesion was defined as both the zone of pallor and the surrounding haemorrhagic border zone, while for the chronic specimens, the ablation lesion was defined as the zone of pallor alone (as there is no surrounding haemorrhagic border zone). The total volume of injury for each animal was calculated by summing the cross-sectional areas and multiplying by the slice thickness. The mean value for the two observers was then taken.

Statistical analysis

Variables are expressed throughout as mean $\pm$ SD, except for voltages, which are expressed as geometric mean and 95% confidence interval (CI). Student's *t*-test for paired data was used to compare pre-ablation,

post-ablation, and chronic CMR segmentations. Student's *t*-test for unpaired data was used to compare pre-ablation, post-ablation, and chronic endocardial voltages. A significance level of $P < 0.05$ was considered statistically significant. Interobserver variability for macroscopic pathological examination was assessed by the intraclass correlation coefficient. Sample size was not determined by a power calculation but was limited by the ability to house a maximum of eight animals for the 2 months following ablation.

Results

Electroanatomical maps and ablation

All 16 animals survived until the end of the protocol and no animals were excluded from analysis due to premature death. Percutaneous

femoral venous access could not be achieved in one animal and a femoral venous cut-down was required. Otherwise, there were no complications during any of the studies.

There were a total of 16 pre-ablation, 16 post-ablation, and 8 chronic electroanatomical maps with an average of 545 ± 400 points (mean point density 40 ± 32 per cm^2). The average time to create a high-density map was 18.5 ± 9.5 min, and the average duration of RF application was 11.6 ± 4.2 min. After ablation, a new atrial activation pattern and double potentials were seen in all 16 animals and also in the 8 chronic animals, confirming completion of the linear intercaval line.

An average of 10 ± 2 axial slices at 4 mm intervals were taken through each voltage map to define the change in voltage 25 mm either side of the centre of the ablation line. The results for all animals were averaged to give summary data for pre-ablation, post-ablation, and chronic pigs, as shown in *Figure 3*.

The mean voltage at the centre of the ablation line was 3.3 mV (95% CI 0.8–9.1) pre-ablation, 0.6 mV (95% CI 0.1–1.5) post-ablation, and 0.3 mV (95% CI 0.1–0.8) chronically. The post-ablation voltages were significantly lower ($P < 0.05$) than the pre-ablation voltages between -19 and $+17$ mm either side of the centre of the ablation line. Chronic voltages were significantly lower ($P < 0.05$) than the pre-ablation voltages between -24 and $+21$ mm. Chronic voltages were significantly lower ($P < 0.05$) than the acute post-ablation voltages between -2 and $+11$ mm.

Cardiac magnetic resonance

There were a total of 16 pre-ablation, 16 post-ablation, and 8 chronic 3D T2W and LGE scans. Example images showing the site of ablation are shown in *Figure 4*. Qualitatively, no appreciable pre-ablation T2W or LGE enhancement was seen in any of the animals, but both T2W and LGE enhancement were seen in all animals post-ablation. Chronically, T2W enhancement had reduced, while LGE enhancement remained.

The summary data for the eight pigs are shown in *Figure 5A* and *B*. For T2W and LGE images, segmented volumes were significantly greater for post-ablation images compared with pre-ablation images.

The summary data for the eight mini-pigs are shown in *Figure 5C* and *D*. For T2W and LGE images, segmented volumes were significantly greater for post-ablation images compared with pre-ablation images. When compared with acute post-ablation images, there was a significant reduction in the segmented volume for chronic T2W images, but no statistical difference for chronic LGE images.

Macroscopic and microscopic examination

Macroscopic photographs of acute and chronic ablation lesions, both immediately after heart explantation and after fixing in formaldehyde, are shown in *Figure 6*. In all animals and all 4 mm cross sections, microscopic histology of acute ablation injury confirmed transmural injury with coagulative necrosis, haemorrhage and interstitial oedema, while chronic histology demonstrated transmural replacement of normal atrial wall with fibrous scar tissue (*Figure 7*).

The mean acute volume of injury measured on the cross sections in the eight pigs was 2.75 ± 1.26 cm^3, while the mean chronic volume of injury in the eight mini-pigs was 1.51 ± 0.53 cm^3. However, when corrected for the difference in atrial area between the pigs and mini-pigs (7.48 ± 0.85 vs. 4.39 ± 1.05 cm^2), there was no significant difference ($P = 0.9$). The interobserver variability for acute and chronic measurements was 0.95 (95% CI 0.69–0.99) and 0.87 (95% CI 0.53–0.97), respectively.
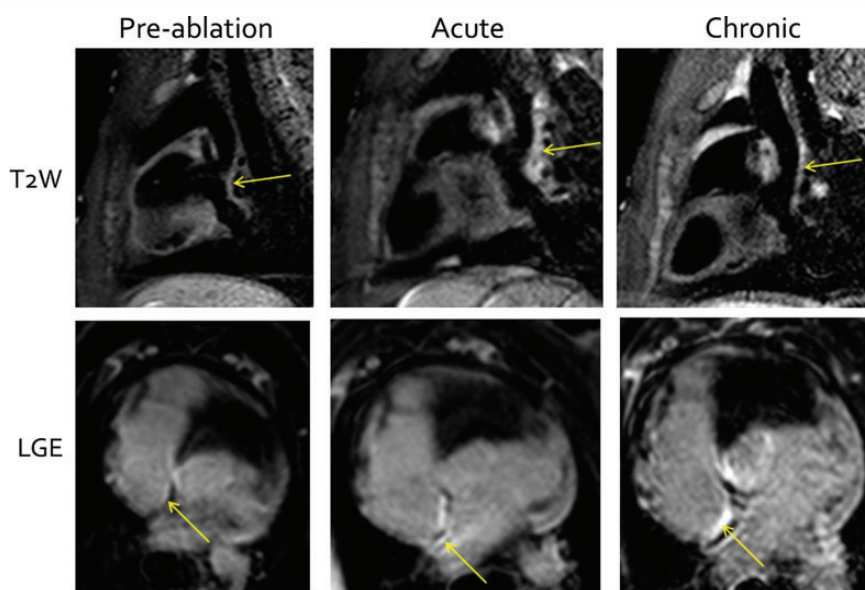
Figure 4 Cardiac magnetic resonance of ablation injury. Sagittal T2-weighted (top row) and axial late gadolinium enhancement (bottom row) cardiac magnetic resonance images pre-ablation (left column), acutely post-ablation (middle column), and chronically (right column). The site of ablation at the posterior right atrial wall is indicated by the arrow.

Figure 5 Segmented cardiac magnetic resonance volumes. Signal intensity thresholds from 0 to 15 standard deviations above a reference SI were applied to the right atrial wall for T2-weighted and late gadolinium enhancement images and a 3D segmentation was created for each threshold. (*A* and *B*) The results for the eight pigs, and (*C* and *D*) the results for the eight mini-pigs. Values in the tables show the statistical comparison within each graph. Dashed lines indicate ±1 SD.

Comparison with cardiac magnetic resonance segmented volumes

When the CMR-segmented volumes were compared with the macroscopic volumes of injury, the SI thresholds that best approximated macroscopic volumes were: 2.3 SD above the mean atrial blood pool SI for LGE post-ablation; 3.3 SD above the mean atrial blood pool SI for LGE chronically; and 14.5 SD above the mean LV myocardium SI for T2W post-ablation (*Figure 8*). Chronically, T2W always underestimated the lesion volume, even at 0 SD above the reference SI.

Discussion

This study was prospectively designed to provide objective T2W and LGE CMR SI and endocardial voltage thresholds for defining acute and chronic atrial ablation injury, by comparison with macroscopic and microscopic pathological examination. The principal findings can be summarized as follows: (i) LGE CMR SI thresholds of 2.3 SD (acutely) and 3.3 SD (chronically) above the mean SI of the atrial blood pool best approximate macroscopic volumes of injury; (ii) T2W CMR overestimates the volume of ablation injury acutely, up to 14.5 SD above the mean SI of the LV myocardium, while T2W
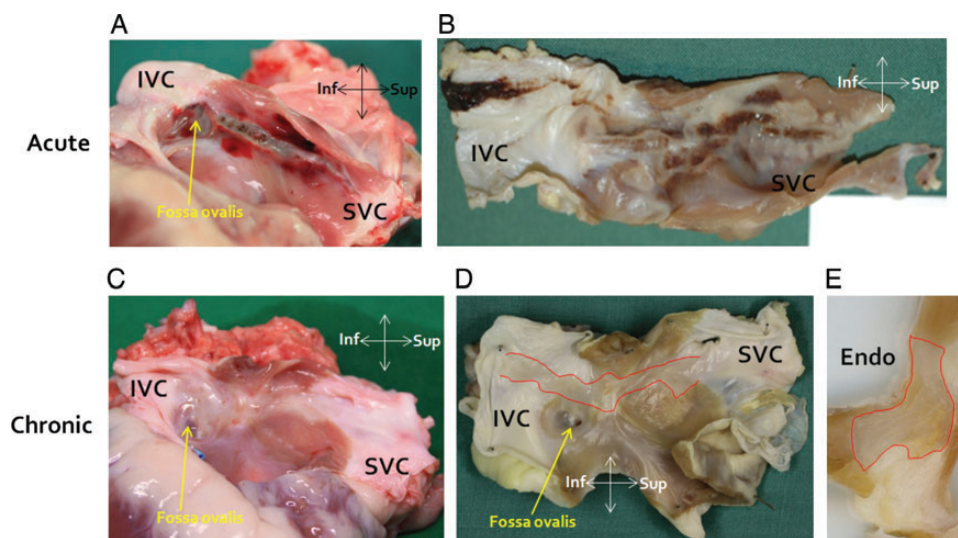
Figure 6 Macroscopic pathology. (*A* and *B*) Macroscopic photographs from animals euthanized acutely after ablation. 'A' is immediately after heart explantation, whereas 'B' is after fixation in formaldehyde. (*C* and *D*) Macroscopic photographs from an animal euthanized 8 weeks after ablation. 'C' is immediately after heart explantation, whereas 'D' is after fixation in formaldehyde (the ablation lesion is outlined in red). (*E*) Cross-section through 'D' with the chronic ablation lesion outlined in red. Inf, inferior; Sup, superior; Endo, endocardial surface.

CMR underestimates the volume of ablation injury chronically regardless of the SI threshold used; (iii) mean endocardial voltage at the centre of a CMR-confirmed linear atrial ablation lesion is 3.3 mV before ablation, 0.6 mV immediately after ablation, and 0.3 mV chronically; and (iv) microscopic examination of a CMR-confirmed ablation line shows transmural coagulative necrosis acutely and transmural fibrosis chronically.

Cardiac magnetic resonance of ablation injury

Several animal studies have shown that ventricular ablation lesions can be acutely visualized with CMR following thermal injury. However, visualizing lesions in the thinner walled atria is inherently more challenging. Even at the current limits of CMR spatial resolution, the atrial wall is covered by only a few voxels and the contrast between acute injury or chronic scar/fibrosis and healthy atrium is less easily visualized than in the ventricle. Published studies investigating atrial CMR lesion measurements and pathological examination are limited and have been in the context of real-time CMR-guided electrophysiology.[13–15] One study showed a correlation between the size of four focal atrial ablation lesions, measured by T2W CMR and macroscopic examination, but only 30% of lesions could be visualized.[14] Another demonstrated a correlation between the size of eight focal atrial and ventricular ablation lesions measured by T2W and LGE CMR and macroscopic examination, with a trend towards larger lesion size measured by T2W CMR.[15] However, only the lesion diameter was measured in these studies—lesion volume was not taken into account. Most recently, investigators demonstrated the ability of CMR to visualize deliberate gaps in acute ablation lesions up to 1.4 mm in size with a strong correlation between gap lengths identified using CMR and gross pathology.[13]

Cardiac magnetic resonance signal intensity thresholds

The aforementioned animal studies used arbitrary SI thresholds/ image windowing to define areas of T2W and LGE enhancement and changes in these values could make a significant difference to the lesion measurements. While studies have suggested CMR SI thresholds to quantify myocardial scar in a range of conditions, including acute and chronic myocardial infarction and hypertrophic cardiomyopathy,[21,22] no studies have attempted to validate similar thresholds for acute or chronic atrial (or ventricular) ablation injury. As a result, a variety of SI thresholds to distinguish between healthy and injured atrial tissue have been used: 2–4 SD above the normal atrial wall SI to quantify LA pre-ablation fibrosis[2] and 3 SD to quantify post-ablation injury.[8,10] In these and indeed any study, an alteration in the threshold would change the quantification.

Atrial endocardial voltage thresholds

Endocardial voltage mapping before catheter ablation for atrial arrhythmias can help to characterize the underlying atrial substrate and identify areas of previous ablation injury.[23] Most commonly, atrial scar is identified by a bipolar voltage of ≤0.05 mV—this threshold originates from the baseline noise in early EAM systems[24] and has been propagated through the literature and clinical practice without published pathological validation. Equally, thresholds to identify 'low voltage', but not scarred, atrial tissue have generally been extrapolated from ventricular studies of post-myocardial infarction scar. In animal models, bipolar voltages of ≤1.0 and ≤0.5 mV best correlated with pathological infarct size.[19,20] In a human study of ischaemic and non-ischaemic cardiomyopathy, authors defined abnormal endocardium as a bipolar electrogram of <1.5 mV and 'densely scarred' endocardium as <0.5 mV.[25]
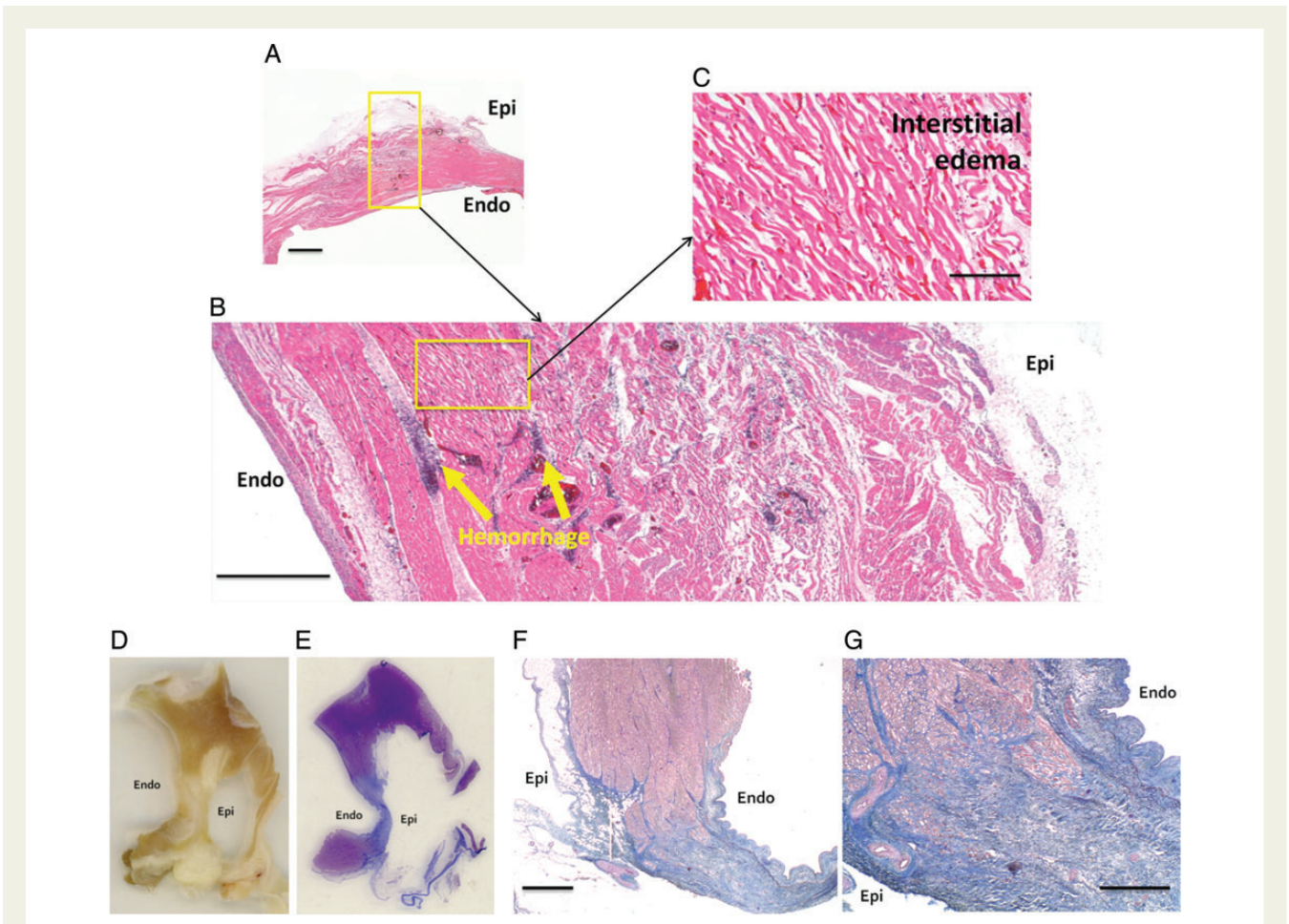
Figure 7 Microscopic histology. (*A−C*) Histology (stained with haematoxylin and eosin) of an acute ablation line at increasing levels of magnification demonstrating transmural injury with coagulative necrosis, haemorrhage, and interstitial oedema. Scale bars in (*A*)−(*C*) are 1 mm, 500 μm, and 100 μm, respectively. Macroscopic cross-sections through a chronic ablation line (*D*—4 mm section after fixation in formaldehyde; *E*—3 μm section after staining with Masson's Trichrome, with which fibrous collagen appears blue). (*F* and *G*) Microscopic histology of a chronic ablation line, stained with Masson's Trichrome, demonstrating transmural replacement of normal atrial wall with fibrous scar tissue. Scale bars in (*F*) and (*G*) are 1 mm and 500 μm, respectively.

In this study, the mean bipolar voltage at the centre of the ablation line was 0.6 mV acutely and 0.3 mV chronically. These values would suggest that using a threshold of ≤0.05 mV to define atrial scar could significantly underestimate the extent of previous ablation injury, perhaps leading to inaccurate interpretation of voltage data and even unnecessary ablation during a redo atrial ablation procedure.

There was a statistically significant reduction in voltage (compared with pre-ablation voltages) almost 2 cm either side of the centre of the line. There are several potential reasons why the area of recorded low voltage may be greater than the actual size of the ablation line: (i) at any point, the measured bipolar voltage depends on the tissue in the surrounding area, even if outside of the zone of histological damage; (ii) when creating an intercaval ablation line in the porcine RA, the catheter sits in a concave groove, such that the contact area may be larger than if perpendicularly opposed to a flat piece

of tissue; (iii) catheter, cardiac, and respiratory motion may cause inaccuracies in the electroanatomical shell.

Pathology of acute and chronic atrial ablation injury

The pathology of acute RF atrial ablation injury in animal models is well established and is characterized by coagulation necrosis,[26] as seen in this study. However, the microscopic features of chronic atrial ablation injury are much less well described, due to the increased complexity in performing recovery animal experiments. Transmural myocardial fibrosis with areas of chronic inflammatory cell infiltration was seen in pigs four weeks after linear non-irrigated ablation in the RA.[27] In open-chest beating heart sheep and dog models of RF ablation, there was replacement of the atrial myocardium with a fibrin and collagen matrix 30 days after ablation.[28,29] In the present study, animals were recovered
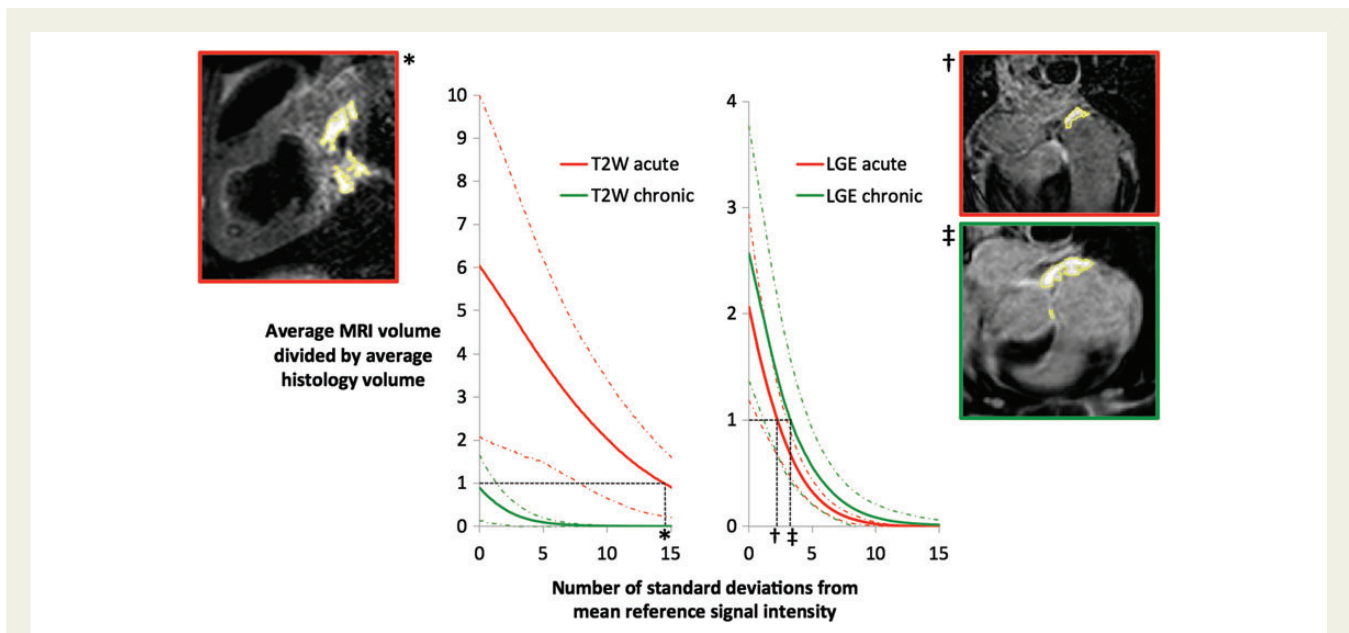
Figure 8 Cardiac magnetic resonance thresholds. Graphs showing the comparison of cardiac magnetic resonance segmented volumes with macroscopic volumes of injury for T2-weighted (left) and late gadolinium enhancement (right). A value of >1 on the *y*-axis suggests that cardiac magnetic resonance is overestimating the macroscopic volume, while a value of <1 suggests underestimation. Thresholds are determined by the intersection with the line *y* = 1. Sample images are included to show the segmentation created (outlined in yellow) at these thresholds. Red and green dashed lines indicate ± 1 SD. *, 14.5 SD, †, 2.3 SD, ‡, 3.3 SD.

for 8 weeks to ensure a representative model of chronic ablation injury and histological findings were in keeping with the aforementioned studies, with transmural fibrous scar.

Limitations

(1) Extrapolation of results to humans is always a potential limitation of animal models. The LA is the predominant target of catheter ablation for AF and so clinical CMR studies have focused on LA ablation. The porcine LA does not closely resemble the human LA, and its structure is not conducive to the reproducible deployment of a linear ablation lesion. For this reason, ablation was performed on the thin posterior RA wall, which is most comparable with the human LA.

(2) The CMR thresholds identified in this study are for the identification of post-ablation injury and are not applicable to quantification of *de novo* atrial fibrosis, for which a specific animal model would be required.

(3) Determining volumes of injury on CMR images and pathological examination are challenging, particularly in the thin-walled atrium. Both require a subjective judgement (to segment the RA wall on CMR and to segment the ablation lesion on pathology), which was reduced as far as possible by the use of two blinded expert observers for each measurement. Furthermore, shrinkage of the pathological specimens may also occur during the preserving process.

(4) Surface coil proximity, sequence parameters, body mass index, haematocrit, renal function, and field strength can all affect T2W and LGE signal intensities. Furthermore, there is currently no consensus on the optimum timing of atrial LGE CMR after contrast administration, or on the choice and dose of contrast agent, which can also affect signal intensity. In this study, these parameters were chosen based on previously published studies of atrial CMR and clinical experience. The clinical applicability of the SI thresholds derived in this study would have to take these considerations into account.

Conclusion

This animal study presents the first histopathological validation of CMR and endocardial voltage mapping to define acute and chronic atrial ablation injury, including SI thresholds that best match histological lesion volumes. The endocardial voltage thresholds defined in this study challenge values currently used clinically in humans. An understanding of these thresholds may allow a more informed assessment of the underlying atrial substrate immediately after ablation and before repeat catheter ablation for atrial arrhythmias, potentially preventing unnecessary ablation.

Supplementary material

Supplementary material is available at *European Heart Journal* online.

References

1. Calkins H, Kuck KH, Cappato R, Brugada J, Camm AJ, Chen SA, Crijns HJ, Damiano RJ Jr, Davies DW, DiMarco J, Edgerton J, Ellenbogen K, Ezekowitz MD, Haines DE, Haissaguerre M, Hindricks G, Iesaka Y, Jackman W, Jalife J, Jais P, Kalman J, Keane D, Kim YH, Kirchhof P, Klein G, Kottkamp H, Kumagai K, Lindsay BD, Mansour M, Marchlinski FE, McCarthy PM, Mont JL, Morady F, Nademanee K, Nakagawa H, Natale A, Nattel S, Packer DL, Pappone C, Prystowsky E, Raviele A, Reddy V, Ruskin JN, Shemin RJ, Tsao HM, Wilber D. 2012 hrs/ehra/ecas expert consensus statement on catheter and surgical ablation of atrial fibrillation. *Heart Rhythm* 2012;**9**:632–696.

2. Oakes RS, Badger TJ, Kholmovski EG, Akoum N, Burgon NS, Fish EN, Blauer JJ, Rao SN, DiBella EV, Segerson NM, Daccarett M, Windfelder J, McGann CJ, Parker D, MacLeod RS, Marrouche NF. Detection and quantification of left atrial structural remodeling with delayed-enhancement magnetic resonance imaging in patients with atrial fibrillation. *Circulation* 2009;**119**:1758–1767.

3. Akoum N, Daccarett M, McGann C, Segerson N, Vergara G, Kuppahally S, Badger T, Burgon N, Haslam T, Kholmovski E, Macleod R, Marrouche N. Atrial fibrosis helps select the appropriate patient and strategy in catheter ablation of atrial fibrillation: A DE-MRI guided approach. *J Cardiovasc Electrophysiol* 2011;**22**:16–22.

4. Peters DC, Wylie JV, Hauser TH, Kissinger KV, Botnar RM, Essebag V, Josephson ME, Manning WJ. Detection of pulmonary vein and left atrial scar after catheter ablation with three-dimensional navigator-gated delayed enhancement MR imaging: initial experience. *Radiology* 2007;**243**:690–695.

5. Knowles BR, Caulfield D, Cooklin M, Rinaldi CA, Gill J, Bostock J, Razavi R, Schaeffter T, Rhode KS. 3-D visualization of acute RF ablation lesions using MRI for the simultaneous determination of the patterns of necrosis and edema. *IEEE Trans Bio-Med Eng* 2010;**57**:1467–1475.

6. Arujuna A, Karim R, Caulfield D, Knowles B, Rhode K, Schaeffter T, Kato B, Rinaldi CA, Cooklin M, Razavi R, O'Neill MD, Gill J. Acute pulmonary vein isolation is achieved by a combination of reversible and irreversible atrial injury after catheter ablation: evidence from magnetic resonance imaging. *Circ Arrhythm Electrophysiol* 2012;**5**:691–700.

7. Badger TJ, Oakes RS, Daccarett M, Burgon NS, Akoum N, Fish EN, Blauer JJ, Rao SN, Adjei-Poku Y, Kholmovski EG, Vijayakumar S, Di Bella EV, MacLeod RS, Marrouche NF. Temporal left atrial lesion formation after ablation of atrial fibrillation. *Heart Rhythm* 2009;**6**:161–168.

8. Badger TJ, Daccarett M, Akoum NW, Adjei-Poku YA, Burgon NS, Haslam TS, Kalvaitis S, Kuppahally S, Vergara G, McMullen L, Anderson PA, Kholmovski E, MacLeod RS, Marrouche NF. Evaluation of left atrial lesions after initial and repeat atrial fibrillation ablation: Lessons learned from delayed-enhancement MRI in repeat ablation procedures. *Circ Arrhythm Electrophysiol* 2010;**3**:249–259.

9. Mahnkopf C, Badger TJ, Burgon NS, Daccarett M, Haslam TS, Badger CT, McGann CJ, Akoum N, Kholmovski E, Macleod RS, Marrouche NF. Evaluation of the left atrial substrate in patients with lone atrial fibrillation using delayed-enhanced MRI: implications for disease progression and response to catheter ablation. *Heart Rhythm* 2010;**7**:1475–1481.

10. McGann CJ, Kholmovski EG, Oakes RS, Blauer JJ, Daccarett M, Segerson N, Airey KJ, Akoum N, Fish E, Badger TJ, DiBella EV, Parker D, MacLeod RS, Marrouche NF. New magnetic resonance imaging-based method for defining the extent of left atrial wall injury after the ablation of atrial fibrillation. *J Am College Cardiol* 2008;**52**:1263–1271.

11. Peters DC, Wylie JV, Hauser TH, Nezafat R, Han Y, Woo JJ, Taclas J, Kissinger KV, Goddu B, Josephson ME, Manning WJ. Recurrence of atrial fibrillation correlates with the extent of post-procedural late gadolinium enhancement: A pilot study. *JACC: Cardiovasc Imaging* 2009;**2**:308–316.

12. Reddy VY, Schmidt EJ, Holmvang G, Fung M. Arrhythmia recurrence after atrial fibrillation ablation: can magnetic resonance imaging identify gaps in atrial ablation lines? *J Cardiovasc Electrophysiol* 2008;**19**:434–437.

13. Ranjan R, Kholmovski EG, Blauer J, Vijayakumar S, Volland NA, Salama ME, Parker DL, Macleod R, Marrouche NF. Identification and acute targeting of gaps in atrial ablation lesion sets using a real time MRI system. *Circ Arrhythm Electrophysiol* 2012;**36**:467–476.

14. Vergara GR, Vijayakumar S, Kholmovski EG, Blauer JJ, Guttman MA, Gloschat C, Payne G, Vij K, Akoum NW, Daccarett M, McGann CJ, Macleod RS, Marrouche NF. Real-time magnetic resonance imaging-guided radiofrequency atrial ablation and visualization of lesion formation at 3 tesla. *Heart Rhythm* 2011;**8**:295–303.

15. Nordbeck P, Hiller KH, Fidler F, Warmuth M, Burkard N, Nahrendorf M, Jakob PM, Quick HH, Ertl G, Bauer WR, Ritter O. Feasibility of contrast-enhanced and nonenhanced mri for intraprocedural and postprocedural lesion visualization in interventional electrophysiology: animal studies and early delineation of isthmus ablation lesions in patients with typical atrial flutter. *Circ Cardiovasc Imaging* 2011;**4**:282–294.

16. Sommer P, Grothoff M, Eitel C, Gaspar T, Piorkowski C, Gutberlet M, Hindricks G. Feasibility of real-time magnetic resonance imaging-guided electrophysiology studies in humans. *Europace* 2013;**15**:101–108.

17. Kim RJ, Fieno DS, Parrish TB, Harris K, Chen EL, Simonetti O, Bundy J, Finn JP, Klocke FJ, Judd RM. Relationship of MRI delayed contrast enhancement to irreversible injury, infarct age, and contractile function. *Circulation* 1999;**100**:1992–2002.

18. Hunter RJ, Jones DA, Boubertakh R, Malcolme-Lawes LC, Kanagaratnam P, Juli CF, Davies DW, Peters NS, Baker V, Earley MJ, Sporton SC, Davies LC, Westwood M, Petersen SE, Schilling RJ. Diagnostic accuracy of cardiac magnetic resonance imaging in the detection and characterization of left atrial catheter ablation lesions: a multicenter experience. *J Cardiovasc Electrophysiol* 2013;**24**:396–403.

19. Callans DJ, Ren JF, Michele J, Marchlinski FE, Dillon SM. Electroanatomic left ventricular mapping in the porcine model of healed anterior myocardial infarction. Correlation with intracardiac echocardiography and pathological analysis. *Circulation* 1999;**100**:1744–1750.

20. Sivagangabalan G, Pouliopoulos J, Huang K, Lu J, Barry MA, Thiagalingam A, Ross DL, Thomas SP, Kovoor P. Comparison of electroanatomic contact and noncontact mapping of ventricular scar in a postinfarct ovine model with intramural needle electrode recording and histological validation. *Circ Arrhythm Electrophysiol* 2008;**1**:363–369.

21. Amado LC, Gerber BL, Gupta SN, Rettmann DW, Szarf G, Schock R, Nasir K, Kraitchman DL, Lima JA. Accurate and objective infarct sizing by contrast-enhanced magnetic resonance imaging in a canine myocardial infarction model. *J Am College Cardiol* 2004;**44**:2383–2389.

22. Flett AS, Hasleton J, Cook C, Hausenloy D, Quarta G, Ariti C, Muthurangu V, Moon JC. Evaluation of techniques for the quantification of myocardial scar of differing etiology using cardiac magnetic resonance. *JACC: Cardiovasc Imaging* 2011;**4**:150–156.

23. Verma A, Wazni OM, Marrouche NF, Martin DO, Kilicaslan F, Minor S, Schweikert RA, Saliba W, Cummings J, Burkhardt JD, Bhargava M, Belden WA, Abdul-Karim A, Natale A. Pre-existent left atrial scarring in patients undergoing pulmonary vein antrum isolation: An independent predictor of procedural failure. *J Am College Cardiol* 2005;**45**:285–292.

24. Jais P, Shah DC, Haissaguerre M, Hocini M, Peng JT, Takahashi A, Garrigue S, Le Metayer P, Clementy J. Mapping and ablation of left atrial flutters. *Circulation* 2000;**101**:2928–2934.

25. Marchlinski FE, Callans DJ, Gottlieb CD, Zado E. Linear ablation lesions for control of unmappable ventricular tachycardia in patients with ischemic and nonischemic cardiomyopathy. *Circulation* 2000;**101**:1288–1296.

26. Huang SK, Bharati S, Graham AR, Lev M, Marcus FI, Odell RC. Closed chest catheter desiccation of the atrioventricular junction using radiofrequency energy – a new method of catheter ablation. *J Am College Cardiol* 1987;**9**:349–358.

27. Gepstein L, Hayam G, Shpun S, Cohen D, Ben-Haim SA. Atrial linear ablations in pigs. Chronic effects on atrial electrophysiology and pathology. *Circulation* 1999;**100**:419–426.

28. Prasad SM, Maniar HS, Schuessler RB, Damiano RJ Jr. Chronic transmural atrial ablation by using bipolar radiofrequency energy on the beating heart. *J Thoracic Cardiovasc Surgery* 2002;**124**:708–713.

29. Prasad SM, Maniar HS, Diodato MD, Schuessler RB, Damiano RJ Jr. Physiological consequences of bipolar radiofrequency energy on the atria and pulmonary veins: a chronic animal study. *Ann Thoracic Surgery* 2003;**76**:836–841; discussion 841-832.